Electrochimica Acta 357 (2020) 136788

Contents lists available at ScienceDirect

Electrochimica Acta

journal homepage: www.elsevier.com/locate/electacta

Note

Avocado oil, coconut oil, walnut oil as true oil phase for ion transfer at nanoscale liquid/liquid interfaces

Ran Chen, Kerui Xu, Mei Shen*

Department of Chemistry, The Beckman Institute for Advanced Science and Technology, University of Illinois at Urbana-Champaign, Urbana, IL 61801, United States

ARTICLE INFO

Article history:
Received 19 May 2020
Revised 10 July 2020
Accepted 16 July 2020
Available online 20 July 2020

Keywords:
ITIES
Nanopipette
Oil
Rate constant
High viscosity

ABSTRACT

The interface between two immiscible electrolyte solutions (ITIES), typically formed between an organic (oil) phase and an aqueous phase, is essential for chemical sensing and for studying various electron transfer and ion transfer reactions. Solvent, as part of ITIES structure, plays critical roles in electrochemical reactions at ITIES. While different kinds of organic phases, including viscous ionic liquid, have been reported, use of true oils as organic phase has rarely been explored. In this study, we introduce true oils, including avocado oil, coconut oil, and walnut oil as new organic solvents for ITIES. We observed well defined potential windows, and sigmoidal cyclic voltammograms for ion transfer. We further measured the ion transfer rate constants at true oil-water interfaces supported at nanopipette of ~20–60 nm in radius. Our study offers additional insights on the effect of solvent viscosity on the ion transfer rate at the liquid/liquid interface, with the viscosity of these true oils being ~ 50–70 times that of 1, 2-dichloroethane. We measured the standard ion transfer rate constants of tetrabutylammonium to be 0.21–0.32 cm / s at these true oil-water interface. This work lays the foundation to expand ITIES platform to explore new reactions, playing critical roles in separation science, chemical sensing, chemical synthesis, catalysis, etc.

1. Introduction

The interface between two immiscible electrolyte solutions (ITIES) have become a powerful platform for chemical sensing and for studying a large variety of electron transfer and ion transfer reactions [1–8], including interfacial catalysis [9–11], nanoparticle synthesis [12,13], neurotransmitter detection [14–22], metal ion detection [23–27], etc. This interface is formed between two liquid solvents of a low (ideally) mutual miscibility, with one solvent being usually water and the other one is a polar solvent (organic phase or oil phase) of a moderate or high dielectric permittivity [28]. Marcus proposed an ion-transfer theory based on the recognition that an ion-transfer reaction involves a mechanism for initiating a desolvation from the initial liquid and concerted solvation by the receiving liquid [1,29]. Solvents as part of ITIES structure [30] plays critical roles in electrochemical reactions at ITIES.

Common organic solvents in ITIES studies include 1,2-dicholoroethane (DCE) [3,5,23,31–33], 1,6-dichlorohexane (DCH) [34–36], dichloromethane (DCM) [37], dichlorobenzene (DCB) [38–40], nitrobenzene (NB) [31,41–45],*o*-nitrophenyloctyl ether (NPOE) [46–48], and benzene [49,50]. At macroITIES or micro ITIES, other kinds of organic solvents have been reported, such as room-temperature ionic liquids [51–54], the lower density organic solvents (i. e. 2-hepatanone, 2-octanone, valeronitrile, caprylonitrile, 2-decanone, 3-nonanone, 5-nonanone), and mixed organic solvents to study the effect of solvent on the potential window and transfer potential [55,56], etc. In contrast to macro- and micro-ITIES, exploring new solvents have been very limited at nanometer-sized ITIES electrodes (nanoITIES), with few studies focusing on ionic liquids [57] and octanol [58]. Here, we introduce true oils including avocado oil, coconut oil, and walnut oil as new solvents for organic phase at ITIES (Fig. 1). This is the first time where these true oils are demonstrated as organic solvents for ITIES electrodes at any size.

Avocado oil, coconut oil, and walnut oil as organic solvents have advantages of low cost, non-toxicity, and easy accessibility. On the other hand, their viscosities are ~ 50–70 times that of DCE [59–61] (Table S4) High viscosity slows down the mass transfer in the oil phase, which further affects the ion transfer across ITIES [29,62]. Girault and Shao studied the effect of viscosity of aqueous phase on ion transfer by adding sucrose to water [18]. Existing studies with viscous organic solvents are mainly about ionic liquids (IL) [51–54,57], where the potential windows of the water/IL interfaces were characterized [51–54] and ion transfer across IL-water interfaces were observed [51–54,57]. Among these studies, Mirkin

* Corresponding author.
E-mail address: mshen233@illinois.edu (M. Shen).

https://doi.org/10.1016/j.electacta.2020.136788
0013-4686/

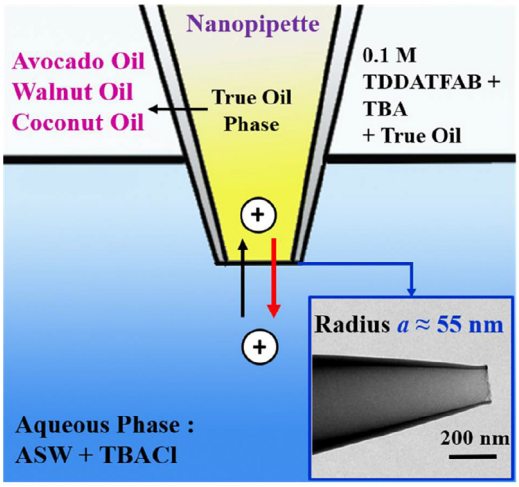

Fig. 1. True oils including avocado oil, walnut oil, coconut oil are introduced as organic solvent for ITIES supported at a nanopipette. Ion transfer kinetics at true oil-water interfaces are studied. Inset: TEM picture of the nanopipette.

and co-workers have successfully determined the TBA transfer kinetics at nano IL-water interface, with rate constants of more than an order of magnitude lower than those obtained at DCE/water interface [57]. Here we introduce a new type of high viscosity organic phase, i.e., avocado oil, coconut oil, and walnut oil. It is unknown how the ion transfer kinetics at avocado oil/water, coconut oil/water, walnut oil /water interfaces are affected by the high viscosity of these oils. We studied the ion transfer kinetics at these true oil-water interfaces supported on nanopipettes of ~ 20–60 nm in radius. This work offers additional insights on the effect of viscosity on the ion transfer rate at the liquid/liquid interface.

We unveiled that these true oil–water interfaces have well-defined potential windows. We observed sigmoidal cyclic voltammograms for ion transfer at nanoscale avocado oil-, coconut oil-, and walnut oil-water interfaces, as expected for nanoelectrodes [62]. Ion transfer at true oil-water interface fit well to Butler–Volmer model, with measured rate constants (up to 0.32 cm/s) not significantly smaller compared to that at DCE / water interface (~1.25 cm/s), considering viscosity of true oils are 50–70 times that of DCE.

2. Experimental

2.1. Reagents and apparatus

Sodium chloride (NaCl) was from EMD Chemicals (Gibbstown, NJ). Potassium chloride (KCl) was from VWR International (Radnor, PA). Magnesium chloride hexahydrate ($MgCl_2 \cdot 6H_2O$) was from Amresco (Solon, OH). Magnesium sulfate ($MgSO_4$) and 4-(2-hydroxyethyl)−1-piperazineethanesulfonic acid (HEPES) were from Fischer Scientific (Pittsburgh, PA). Calcium chloride dihydrate ($CaCl_2 \cdot 2H_2O$), tetradodecylammonium (TDDA) chloride, tetrabutylammonium chloride (TBACl), 1, 2-dichloroethane (DCE), *N, N*-dimethyltrimethylsilylamine, sodium sulfate (Na_2SO_4) were purchased from Sigma-Aldrich (St. Louis, MO). Potassium tetrakis(pentafluorophenyl) borate (TFAB) was purchased from Boulder Scientific Company (Mead, CO). Coconut oil was purchased from Ventura Foods LLC (Brea, CA), walnut oil was purchased from AAK UK Ltd (Hull, England), and avocado oil was purchased from Primal Nutrition LLC (Oxnard, CA). All the aqueous solution was made with 18.3 MΩ cm deionized water. We used artificial seawater (ASW) containing the following: 460 mM NaCl, 10 mM KCl. 10 mM $CaCl_2$, 22 mM $MgCl_2$, 26 mM $MgSO_4$ and 10 mM HEPES (pH 7.8) in 18.3 MΩ cm deionized water as the aqueous solution. The TFAB salt of TDDA (TDDATFAB) was prepared by metathesis as reported previously [20].

Nanopipette electrode fabrication, characterization and electrochemical measurements. The nanoITIES electrodes were fabricated using procedures reported in recent work [19,20,22,63–67]. Briefly, nanopipettes of 20–60 nm radius were prepared by laser pulling quartz capillaries (Sutter Instrument Co., Novato CA; 1 mm outer diameter, 0.7 mm inner diameter, 7.5 cm length) using a P-2000 Laser Puller (Sutter Instruments Novato, CA). The glass surface of the nanopipettes was treated via silanization reaction with *N, N*-dimethyltrimethylsilylamine to convert glass surface from hydrophilic into hydrophobic, thus ensuring the formation of stable oil-water interfaces at the orifice of the nanopipette. The nanoITIES pipette was backfilled with an oil solution of 0.1 M TDDATFAB dissolved in different oil solvents with a 10 µL Hamilton syringe. The filling solution was forced to the nano-tip using gentle vibrations. A Pt wire was inserted into the filled pipette as reported in recent work [19,20,22,65,68]. The nanoITIES pipette was placed in ASW. ASW was used as the aqueous solution because it is the biological cellular medium for our commonly used neuronal model, *Aplysia californica* [63,64], and by studying ion transfer in this media, future biological work related to ASW can be facilitated. The radius of the nanopipettes was calculated from the TBA transfer current using Eq. (2). A Transmission Electron Microscope (TEM) (Philips CM200, FEI Co., Hillsboro, OR) was also used to confirm the radius of the nanopipettes under a 120 kV electron beam.

All electrochemical measurements were performed using either a CHI 920D potentiostat (CHI Instruments, Austin, TX) or a CHI760E potentiostat (CHI Instruments, Austin, TX). We used cyclic voltammetry (CV) to measure the potential window and to study the ion transfer at these new interfaces. We used a two-electrode configuration [19,20,22,65,68,69], where a potential was applied between the inner Pt wire and the outer Ag/AgCl reference electrode. Negative potential is for positive ion transfer from water to oil, seen as positive current, as commonly reported [3,19,20,22,36,57,66,68,69].

Analysis of the onset potential in the positive direction, E_{pos}, and in the negative potential, E_{neg}. To make a quantitative comparison between the potential windows of different true oil-ASW interfaces, TBA was added to ASW as the internal standard at each oil-ASW interface, and the potential was reported with respect to the half-wave transfer potential of TBA, $E_{1/2,TBA}^{oil}$. As shown in Scheme 1, to determine E_{pos} and E_{neg} in the background CVs, the baseline current (i_{base}) and capacitive current (i_c) were first determined from the capacitive current region of the CV. i_{base} is defined as the average current of the forward and reverse scan in the capacitive current region. i_c is half of the absolute current gap between the forward and reverse scan at capacitive current re-

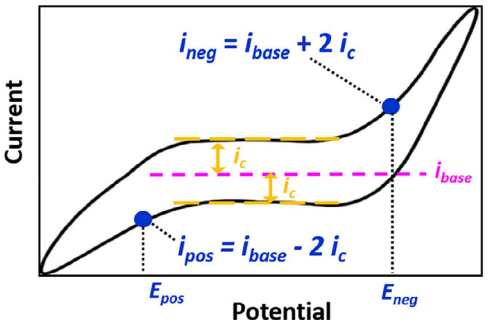

Scheme 1. Determination of the onset potentials. The baseline current(i_{base}), the capacitive current(i_c), the onset current in the positive direction(i_{pos}), and the onset current in the negative direction(i_{neg}) were defined. The potentials at i_{pos} and i_{neg} are the onset potential in the positive direction, E_{pos}, and in the negative direction, E_{neg}, respectively.

gion. The onset current in the positive direction, i_{pos}, is defined as $i_{pos} = i_{base} - 2 \times i_c$ and the potential corresponding to i_{pos} in the lower capacitive current trace is E_{pos}. The onset current in the negative direction, i_{neg}, is defined as $i_{neg} = i_{base} + 2 \times i_c$ and the potential corresponding to i_{neg} in the upper capacitive current trace is E_{neg}.

2.2. Kinetics analysis of ion transfer across the oil/water interface

Overview. The kinetics of the TBA transfer across the oil / water interface was measured at nanoITIES and analyzed using the reported method [70,71]. Experimentally speaking, the nanopipettes were filled with an oil phase containing 5 mM (or 0.5 mM) TBA and the aqueous phase contained 2 mM TBA. The voltammogram for the ion transfer was collected and then analyzed to determine the kinetic parameters. We include below the methodologies described in the original work by Mirkin and Amemiya groups [70,71], with description modified to fit our study.

To extract the kinetic parameters from experimental steady-state voltammograms, we employed the following equation:

$$\frac{i}{i_{ing}} = \frac{1}{\frac{m_{ing}}{m_{eg}} + \frac{m_{ing}}{k_b} + \frac{k_f}{k_b}} \left(\frac{k_f}{k_b} - \frac{c_1}{c_2} \right) \tag{1}$$

We describe in the following subsections about each of the parameters included in the above equation.

The limiting current of the ingress process, i_{ing}. i_{ing} corresponds to the ion transfer from the external solution (i.e. aqueous phase) into the nanopipette. It can be described as:

$$i_{ing} = 4xzFD_2c_2a \tag{2}$$

where z is the number of charges of the ion, D_2 is the diffusion coefficient of the ion in the outer aqueous phase, c_2 is the bulk concentration of the ion in the outer aqueous solution, F is Faraday constant, and x is a parameter related to the RG of the nanopipette ($RG = r_g$ / a, r_g and a are the outer radii and inner radii of the nanopipette) [72]. Here, $RG = 1.4$, and $x = 1.23$.

Mass transfer coefficient of ingress (m_{ing}) and egress (m_{eg}). m_{ing} can be calculated using expression below, where all parameters have been defined above.

$$m_{ing} = \frac{4xD_2}{\pi a} \tag{3}$$

For m_{eg}, it is described in Eq. (4),

$$m_{eg} = \frac{4f(\theta)D_1}{\pi a} \tag{4}$$

where D_1 is the diffusion coefficient in the oil phase, $f(\theta)$ is a tabulated function of the tip taper angle, θ [73]. However, in our experiments D_1 is unknown for food oils, thus calculating m_{eg} using Eq. (4) directly can be difficult. As an alternative method to calculate m_{eg}, we rearranged Eq. (4) by replacing $f(\theta)$ D_1 based on Eq. (6) to generate new Eq. (5). This way, we calculated m_{eg} without knowing the exact value of D_1:

$$m_{eg} = \frac{4f(\theta)D_1}{\pi a} = \frac{i_{eg}}{zFC_1a^2} \tag{5}$$

In Eq. (5), all parameters can be obtained as described above, except i_{eg} and c_1, which is defined in next section.

The limiting current of egress process, i_{eg}. i_{eg} corresponds to the ion transfer from the internal solution (i.e. oil phase) to the outer aqueous solution. It can be described as:

$$i_{eg} = 4f(\theta)zFD_1c_1a \tag{6}$$

where D_1 and c_1 are the diffusion coefficient and bulk concentration in the internal oil phase, respectively, and $f(\theta)$ is a tabulated function of the tip taper angle, θ [73].

Table 1
Parameters used for simulation of ion transfer voltammograms.

Constant	Value	Definition
z	1	Number of charges
F	96,485 C/mol	Faraday constant
R	8.314 J/mol K	Gas constant
T	298 K	Temperature
c_1	5.0 (or 0.5) mM	Ion (TBA) concentration in oil phase
c_2	2.0 mM	Ion (TBA) concentration in aqueous phase
D_2	5.1×10^{-6} cm^2/s [65]	Diffusion coefficient of the ion in aqueous phase

Heterogeneous ion transfer rate constant k_f and k_b. k_f and k_b are the heterogeneous ion transfer rate constant of the ingress process and egress process, respectively. They are described by the Butler-Volmer model [28]:

$$k_f = k^0 \exp\left[\frac{-\alpha zF}{RT} \left(\Delta\varphi - \Delta\varphi_i^{0'} \right) \right] \tag{7}$$

$$k_b = k^0 \exp\left[\frac{(1-\alpha)zF}{RT} \left(\Delta\varphi - \Delta\varphi_i^{0'} \right) \right] \tag{8}$$

where k^0 is the standard heterogeneous ion transfer rate constant, R is the gas constant, T is temperature, α is the transfer coefficient, $\Delta\varphi$ is the Galvani potential difference between the two liquid phases, and $\Delta\varphi_i^{0'}$ is the formal transfer potential of the ion. The formal potential can be determined from the potential value at zero current in the voltammogram, $\Delta\varphi_{eq}$, as described by:

$$\Delta\varphi_{eq} = \Delta\varphi_i^{0'} + \frac{RT}{zF} ln \frac{c_2}{c_1} \tag{9}$$

Constants and parameters used for analysis Table 1. The constants and parameters used in Eqs. (1)-(9) are listed in.

Simulation of the experimental data to determine α and k^0. We used Eq. (1) to generate the theoretical voltammogram to fit experimental voltammograms. The parameters in Eq. (1) are described in equations (2) through (9) as detailed above. More specifically, we first obtained i_{ing} and i_{eg} from the experimental voltammograms, which were then used in Eq. (2) to calculate a, and in Eqs. (3) and (5) to obtain m_{ing} and m_{eg}, respectively. i_{ing}, i_{eg}, m_{ing}, m_{eg}, and the parameters listed in Table 1 were constants for a given experimental voltammogram. Then we determined $\Delta\varphi_{eq}$ from the experimental voltammogram and calculated $\Delta\varphi_i^{0'}$ based on Eq. (9). We further calculated k_f and k_b using Eqs. (7) and (8) at the corresponding potential, $\Delta\varphi$, of the experimental voltammogram; initially, we used arbitrary preset values of α and k^0 (e.g. α of 0.5 and k^0 of 1.0 cm/s), which will be adjusted until the best fit between theoretical and experimental voltammograms. Finally, we plotted the current i as a function of $\Delta\varphi$ using Eq. (1) to generate the theoretical voltammogram, which will be fit to the experimental voltammogram to determine α and k^0 values.

3. Results and discussion

3.1. Potential window of coconut oil-, water, avocado oil-, water and walnut oil-, water interfaces

We measured the potential windows of these true oil-water interfaces, with the cell diagram shown below:

Cell 1 (oil: avocado oil, coconut oil, walnut oi):

Pt | 0.1 M TDDATFAB (electrolyte) + oil || artificial sea water (ASW) | AgCl | Ag

Nanopipette Outer aqueous solution

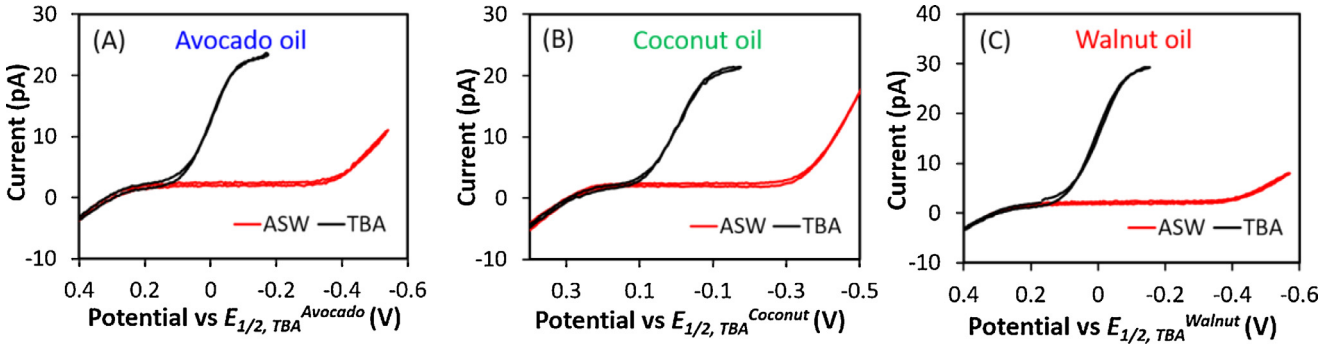

Fig. 2. The background CVs (red curve) at (A) avocado oil-, (B) coconut oil- and (C) walnut oil- ASW interfaces. Cyclic voltammograms of TBA transfer were shown as black curves. TBA concentrations were 5 mM in the aqueous phase only. Similar results were observed from at least three different pipettes for each of the oil phases. The potential was reported with respect to the half wave transfer potential of TBA across the corresponding true oil-ASW interface, $E_{1/2,TBA}^{oil}$. Pipettes of different sizes were used in A, B and C. Scan rate: 25 mV/s. . (For interpretation of the references to color in this figure legend, the reader is referred to the web version of this article.)

We present in Fig. 2 the background cyclic voltammograms (CVs) at nano avocado oil-, coconut oil-, walnut oil-ASW interfaces, respectively. In Fig. 2, at each true oil-ASW interface, the background CVs were plotted with respect to the half wave transfer potential of TBA, $E_{1/2,TBA}^{oil}$.

To study the potential windows of different oils quantitatively, we compared E_{neg} and E_{pos} of each voltammogram, with E_{neg} being the onset potential at the negative direction and E_{pos} being the onset potential at the positive direction of the CVs. The procedure of determining E_{neg} and E_{pos} are detailed in the Experimental section. E_{neg} and E_{pos} for avocado oil-, coconut oil-, walnut oil- and DCE-ASW interfaces are summarized in Table S3. Less negative E_{neg} for avocado oil, coconut oil, and walnut oil was observed compared to DCE with ΔE_{neg} being 0.272 (± 0.022) V, 0.320 (± 0.026) V and 0.295 (± 0.038) V, respectively. This suggests that coconut, walnut, and avocado oils might be less favorable for the detection of certain cations. A big advantage could be easier detection of cations existing in ASW. Avocado oil, coconut oil, and walnut oil all have more positive E_{pos} compared to DCE, with ΔE_{pos} being 0.160 (± 0.031) V, 0.198(± 0.019) V and 0.136 (± 0.022) V, respectively. This extended potential window at the positive direction could enable the detection of anion species that otherwise would be difficult in DCE. Additionally, in the supporting information and Fig. S2, we showed one example to demonstrate that the earlier onset positive potential (E_{pos}) at the DCE-ASW interface affects the CV measurements. The difference in E_{pos} and E_{neg} among the three oils might be related to the composition of oils. The composition of the oils in terms of saturated fat, mono-unsaturated fat and poly-unsaturated fat provided by the vendors was shown in Table S1. According to Table S1, coconut oil is largely composed of saturated fatty acids, while avocado oil and walnut oil are largely composed of unsaturated fatty acids. These saturated fatty acids have a higher solubility in water compared to the unsaturated fatty acids. The fatty acid compositions are also consistent with the reported chemical composition of the true oils measured using gas-chromatography, as summarized in Table S2.

3.2. Cyclic voltammograms of ion transfer at coconut oil-, walnut oil- and avocado oil–water interfaces

While we have shown that well-defined potential windows can be achieved in coconut oil, walnut oil and avocado oil, it is unknown if ion transfer (e.g. widely used standard compound in ITIES studies, TBA) occurs on these true oil–water interfaces. Furthermore, if ion transfer does occur, would similar steady-state current be achieved for TBA transfer at true oil–water interfaces compared to a commonly used DCE-Water interface? To answer these unknown questions, we prepared nanoITIES electrodes from a pair of nanopipette by pulling the same glass capillary, with each of the pairs denoted as a and b. Then we filled pipette-a with true oil (electrode-a) and the other corresponding pair (electrode-b) with 1, 2-DCE to prepare two ITIES electrodes with the same size. Then we measured TBA transfer using electrode-a to study its transfer at oil–water interfaces and compared the steady-state current to that measured at electrode-b. The cell diagram for each true oil is shown below unless otherwise noted. In cell 2, true oils are avocado oil, walnut oil, coconut oil; $x = 5.0$ for coconut oil, and $x = 0.5$ for avocado and walnut oil. $x = 0.5$ was used for avocado and walnut oils due to the lower solubility of TBA in these oils.

Cell 2:

Pt | 0.1 M TDDATFAB + x mM TBACl + true oil || ASW + 2.0 mM TBACl | AgCl | Ag

Nanopipette Outer aqueous solution

Ion transfer CVs were shown in Fig. 3, where the transfer of TBA was observed in all the three oil-ASW interfaces. We observed sigmoidal shapes for TBA transfer voltammograms at these oil-water interfaces using electrode-a, as expected for nanoelectrodes [62]. To analyze if the diffusion limiting current value corresponds to the size of the nanoITIES electrode, we also measured the CVs using the corresponding electrode-b at the DCE-ASW interface (Figs. S1A, 1B and 1C). Similar steady state currents were observed in electrode-a and electrode-b. For example, a steady-state current of ~25 pA was measured at coconut-water interface (electrode-a, Fig. 3B) and ~ 27 pA at DCE-water interface (electrode-b, Fig. S1B). Considering similar tip radius for a pair of nanopipettes and the same TBA concentrations, this result indicates that steady state current as expected from theory was measured at these true oil–water interfaces (Eq. (2) in experimental section). We further examined the ion transfer kinetics at avocado oil-ASW, coconut oil-ASW, walnut oil-ASW interfaces in the next section.

3.3. Kinetic analysis of ion transfer at coconut oil-, walnut oil- and avocado oil-water interfaces

The theory and procedure for determining the ion transfer kinetics was detailed in the experimental section, where TBA was added to both the oil filling solution and aqueous phase. We first measured the cyclic voltammogram corresponding to the ingress of TBA into the pipette and the egress of TBA out of the pipette (Fig. 1). Then we further simulated the experimental voltammograms using theory to obtain the kinetic parameters, i. e. transfer coefficient, α, and standard ion transfer rate constant, k^0. We confirmed that our experimental setup works well using the reported method [70,71] to determine kinetic parameters by obtaining DCE kinetics similar to literature (Fig. S3). α of 0.45 ± 0.03 and k^0 of

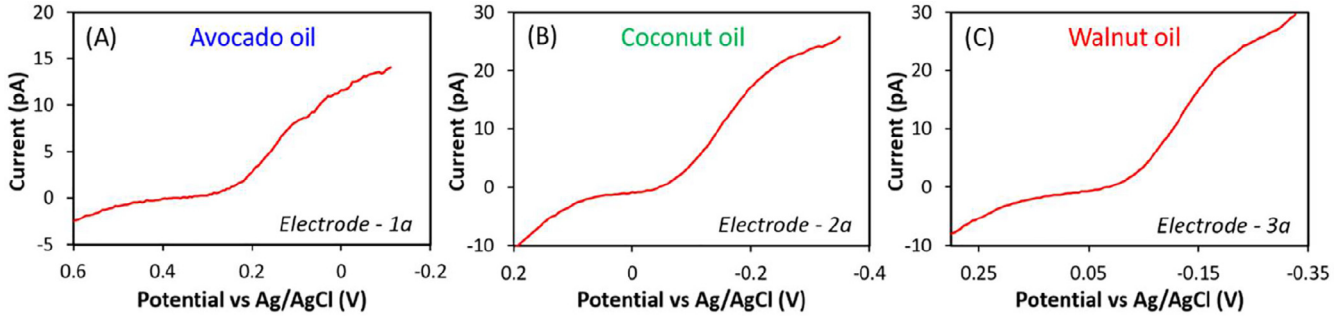

Fig. 3. Ion transfer cyclic voltammograms at avocado oil-ASW (A), coconut oil-ASW (B) and walnut oil-ASW (C) interfaces using electrode-a. Ion: TBA. The forward scans of the cyclic voltammograms were plotted. Scan rates: 25 mV/s.

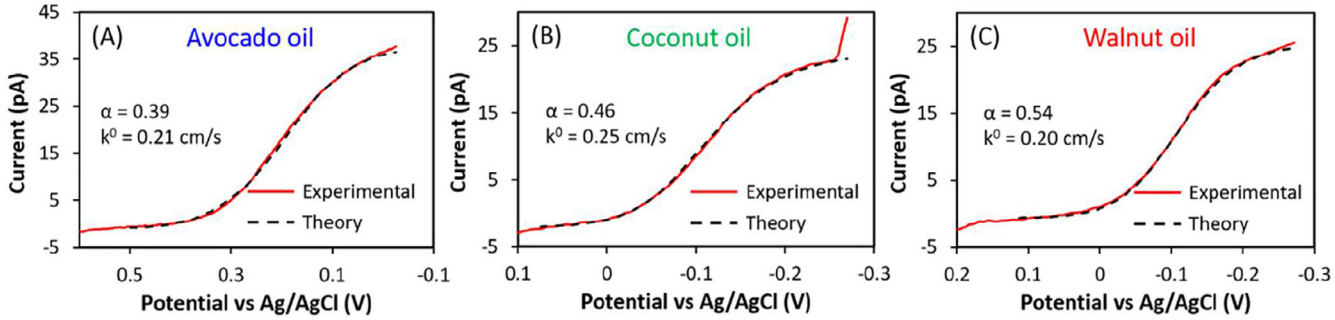

Fig. 4. Determination of the ion transfer kinetics from voltammograms at avocado oil-ASW (A), coconut oil-ASW (B) and walnut oil-ASW (C) interfaces, by fitting the experimental voltammograms (red solid lines) to the theoretical voltammograms (black dashed lines). The forward scan of the voltammogram was plotted. Ion: TBA. Scan rates: 25 mV/s. In Fig. A, TBA concentration in the aqueous solution was 5 mM. (For interpretation of the references to color in this figure legend, the reader is referred to the web version of this article.)

Table 2
Kinetic parameters at novel true oil-water interfaces for TBA transfer.

Oil	Transfer coefficient α	Standard ion transfer rate constant k^0 (cm/s)
Avocado oil	0.40 ± 0.03 ($n = 3$)	0.26 ± 0.05 ($n = 3$)
Coconut oil	0.46 ± 0.02 ($n = 3$)	0.21 ± 0.04 ($n = 3$)
Walnut oil	0.55 ± 0.03 ($n = 2$)	0.32 ± 0.14 ($n = 2$)
DCE	0.45 ± 0.03 ($n = 9$)	1.25 ± 0.38 ($n = 9$)

1.25 ± 0.38 cm/s were measured for TBA transfer at DCE-water interface, which was similar to that reported in the literature for TBA [68] as well as α and k^0 measured for tetraethylammonium (TEA) and tetramethylammonium (TMA) at DCE-water interface [69].

Representative experimental voltammograms (red solid curve) for kinetics analysis at avocado oil-, coconut oil-, walnut oil-ASW interfaces were shown in Fig. 4. These experimental voltammograms fit the simulated voltammograms (black dashed curves). We further determined α and k° from the best fitting. The averaged transfer coefficients and standard ion transfer rate constants for TBA transfer at these true oil-ASW interfaces were summarized in Table 2. Measured transfer coefficients at avocado oil-, coconut oil- and walnut oil–water interfaces ranges from 0.4 to 0.6, as expected for the typical electrochemical ITIES system [68,69,74–76]. k° for TBA transfer at avocado oil-, coconut oil- and walnut oil-water interfaces were 0.26 ± 0.05 cm/s, 0.21 ± 0.04 cm/s and 0.32 ± 0.14 cm/s, respectively.

These k^0 values for TBA transfer at these true oil-water interfaces were smaller compared to that at DCE-water interface; however, they appear to be slightly larger than k^0 at water-ionic liquid interface ($k^0 = 0.12 \pm 0.02$ cm/s) [57]. One possible explanation is the difference in viscosity (Table S4). It has been proposed that higher viscosity leads to a slower k^0 due to a slower diffusion across the boundary layer [18,57]. Based on the slow interfacial diffusion model [77,78], a boundary layer occurs when the two phases (water and oil) are mixed, and $k^0 = D_i / \Delta x$, where D_i and Δx are the diffusion coefficient within and the thickness of the boundary layer. Coconut, walnut, and avocado oils have higher viscosity (a smaller D_i), thus a smaller k^0. A second possible explanation for the difference in k^0 values could be related to variation in solvation energy changes when TBA transfer from water to true oil phases compared to DCE [29,30,79], considering ion-transfer theory proposed by Marcus that an ion-transfer reaction involves a desolvation from the initial liquid and concerted solvation by the receiving liquid. As shown in Table S2, these true oils have different solubility in water compared to DCE in water.

4. Conclusion

New types of true oils, including avocado oil, coconut oil, and walnut oil, are presented for the first time as new organic solvents for nanoITIES studies. We have successfully observed ion transfer (IT) at these new oil–water interfaces. At the nano true oil–water interface, sigmoidal cyclic voltammograms with diffusion limiting current aligning with the theory were observed. We measured the IT rate constants at these new true oil-water interfaces. Despite the high viscosity of the true oils, IT kinetics at the true oil–water interfaces fit the theory based on the Butler–Volmer model. Rate constants of IT at true oil–water interfaces (0.21–0.32 cm/s) are only slightly smaller than that at DCE-water interfaces (1.25 cm/s), while its viscosity is 50–70 times higher. Furthermore, these true oil–water interfaces have distinguished potential windows. Our work lays the foundation for future work in exploring true food oils as a new organic phase in the field of ion transfer and beyond, impacting various fields of chemical sensing, catalysis, separation, and chemical synthesis.

Declaration of Competing Interest

There are no conflicts to declare.

CRediT authorship contribution statement

Ran Chen: Methodology, Investigation, Formal analysis, Writing - original draft. **Kerui Xu:** Investigation, Formal analysis, Writing - original draft. **Mei Shen:** Conceptualization, Methodology, Formal analysis, Writing - review & editing, Supervision, Project administration, Funding acquisition.

Acknowledgments

The TEM measurements were carried out in The Beckman Institute for Advanced Science and Technology.

The research reported in this publication was supported by the National Science Foundation under a CAREER award (CHE 19-45274), and University of Illinois at Urbana-Champaign to M. Shen.

Supplementary materials

Supplementary material associated with this article can be found, in the online version, at doi:10.1016/j.electacta.2020.136788.

References

[1] H.H. Girault, Electrochemistry at Liquid/Liquid Interfaces, in: A.J. Bard, G. Cynthia (Eds.), Electroanalytical Chemistry: A series of Advances, 23, CRC Press, Taylor&Francis Group, Boca Raton, FL, 2010.
[2] P.L. Vanysek, L.B. Ramirez, Interface between two immiscible liquid electrolytes: a review, J. Chil. Chem. Soc. 53 (2008) 1455–1463.
[3] Y. Shao, M.V. Mirkin, Voltammetry at micropipet electrodes, Anal. Chem. 70 (1998) 3155–3161.
[4] S. Amemiya, J. Kim, A. Izadyar, B. Kabagambe, M. Shen, R. Ishimatsu, Electrochemical sensing and imaging based on ion transfer at liquid/liquid interfaces, Electrochim. Acta 110 (2013) 836–845.
[5] G. Taylor, H.H. Girault, Ion transfer reactions across a liquid—Liquid interface supported on a micropipette tip, J. Electroanal. Chem. 208 (1986) 179–183.
[6] S. Liu, Q. Li, Y. Shao, Electrochemistry at micro-and nanoscopic liquid/liquid interfaces, Chem. Soc. Rev. 40 (2011) 2236–2253.
[7] A. Berduque, A. Sherburn, M. Ghita, R.A.W. Dryfe, D.W.M. Arrigan, Electrochemically modulated liquid– liquid extraction of ions, Anal. Chem. 77 (2005) 7310–7318.
[8] A. Izadyar, Stripping voltammetry at the interface between two immiscible electrolyte solutions: a review paper, Electroanalysis 30 (2018) 2210–2221.
[9] Y. Shao, M. Mirkin, J. Rusling, Liquid/liquid interface as a model system for studying electrochemical catalysis in microemulsions. Reduction of trans-1,2-dibromocyclohexane with vitamin B12, J. Phys. Chem. B 101 (1997) 3202–3208.
[10] A.N.J. Rodgers, R.A.W. Dryfe, Oxygen reduction at the liquid–liquid interface: bipolar electrochemistry through adsorbed graphene layers, Chem. Electro. Chem. 3 (2016) 472–479.
[11] S. Rastgar, M. Pilarski, G. Wittstock, A porlarized liquid-liquid interface meets visible light-driven catalytic water oxidation, Chem. Commun. 52 (2016) 11382–11385.
[12] G.C. Gschwend, E. Smirnov, P. Peljo, H.H. Girault, Electrovariable gold nanoparticle films at liquid–liquid interfaces: from redox electrocatalysis to Marangoni-shutters, Faraday Disc 199 (2017) 565–583.
[13] A.N.J. Rodgers, S.G. Booth, R.A.W. Dryfe, Particle deposition and catalysis at the interface between two immiscible electrolyte solutions (ITIES): a mini-review, Electrochem. Comm. 47 (2014) 17–20.
[14] D. Arrigan, M. Ghita, V. Beni, Selective voltammetric detection of dopamine in the presence of ascorbate, Chem. Comm. 6 (2004) 732–733.
[15] V. Beni, M. Ghita, D. Arrigan, Cyclic and pulse voltammetric study of dopamine at the interface between two immiscible electrolyte solutions, Biosens. Bioelectron. 20 (2005) 2097–2103.
[16] D. Zhan, S. Mao, Q. Zhao, Z. Chen, H. Hu, P. Jing, M. Zhang, Z. Zhu, Y. Shao, Electrochemical investigation of dopamine at the water/1, 2-dichloroethane interface, Anal. Chem. 76 (2004) 4128–4136.
[17] V. Marecek, Z. Samec, Electrolysis at the Interface between two immiscible electrolyte solutions: determination of acetylcholine by differential pulse stripping voltammetry, Anal. Lett. 14 (1981) 1241–1253.
[18] Y. Shao, H.H. Girault, Kinetics of the transfer of acetylcholine across the water+ sucrose/1, 2-dichloroethane interface: a comparison between ion transport and ion transfer, J. Electroanal. Chem. 282 (1990) 59–72.
[19] M.L. Colombo, S. McNeil, N. Iwai, A. Chang, M. Shen, Electrochemical detection of dopamine via assisted ion transfer at nanopipet electrode using cyclic voltammetry, J. Electrochem. Soc. 163 (2016) H3072–H3076.
[20] M. Colombo, J. Sweedler, M. Shen, Nanopipet-based liquid–liquid interface probes for the electrochemical detection of acetylcholine, tryptamine, and serotonin via ionic transfer, Anal. Chem 87 (2015) 5095–5100.
[21] M. Shen, M. Colombo, Electrochemical nanoprobes for the chemical detection of neurotransmitters, Anal. Methods 7 (2015) 7095–7105.
[22] N.T. Iwai, M. Kramaric, D. Crabbe, Y. Wei, R. Chen, M. Shen, GABA detection with Nano-ITIES pipet electrode: a new mechanism, Water/DCE–octanoic acid interface, Anal. Chem 90 (2018) 3067–3072.
[23] T.J. Stockmann, A. Montgomery, Z.J. Ding, Determination of alkali metal ion transfers at liquid| liquid interfaces stabilized by a micropipette, Electroanal. Chem. 684 (2012) 6–12.
[24] D. Zhan, X. Li, W. Zhan, F. Fan, A.J. Bard, Scanning electrochemical microscopy. 58. Application of a micropipet-supported ITIES tip to detect Ag^+ and study its effect on fibroblast cells, Anal. Chem. 79 (2007) 5225–5231.
[25] U. Nestor, H. Wen, G. Girma, Z. Mei, W. Fei, Y. Yang, C. Zhang, D. Zhan, Facilitated Li^+ ion transfer across the water/1, 2-dichloroethane interface by the solvation effect, Chem. Comm. 50 (2014) 1015–1017.
[26] Y. Shao, B. Liu, M.V. Mirkin, Studying ionic reactions by a new generation/collection technique, J. Am. Chem. Soc. 120 (1998) 12700–12701.
[27] F.O. Laforge, P. Sun, M.V. Mirkin, Shuttling mechanism of ion transfer at the interface between two immiscible liquids, J. Am. Chem. Soc. 128 (2006) 15019–15025.
[28] Z. Samec, Electrochemistry at the interface between two immiscible electrolyte solutions (IUPAC Technical Report), Pure. Appl. Chem. 76 (2004) 2147–2180.
[29] R.A. Marcus, On the theory of ion transfer rates across the interface of two immiscible liquids, J. Chem. Phys. 113 (2000) 1618–1629.
[30] G.C. Gschwend, A. Olaya, P. Peljo, H.H. Girault, Structure and reactivity of the polarised liquid–liquid interface, Curr. Opin. Electrochem. 19 (2020) 137–143.
[31] B. Hundhammer, T. Solomon, Determination of standard Gibbs energies of ion partition between water and organic solvents by cyclic voltammetry: part I, J. Electroanal. Chem. Interfacial Electrochem. 157 (1983) 19–26.
[32] Z. Samec, A.R. Brown, L.J. Yellowlees, H.H. Girault, K. Base, Photochemical ion transfer across the interface between two immiscible electrolyte solutions, J. Electroanal. Chem. 259 (1989) 309–313.
[33] Z. Ding, R.G. Wellington, P.-.F. Brevet, H.H. Girault, Differential cyclic voltabsorptometry and chronoabsorptometry studies of ion transfer reactions at the water| 1, 2-dichloroethane interface, J. Electroanal. Chem. 420 (1997) 35–41.
[34] E.A. de Eulate, J. Strutwolf, Y. Liu, K. O'Donnell, D.W.M. Arrigan, An electrochemical sensing platform based on liquid–liquid microinterface arrays formed in laser-ablated glass membranes, Anal. Chem. 88 (2016) 2596–2604.
[35] Y. Liu, J. Strutwolf, D.W.M. Arrigan, Ion-transfer voltammetric behavior of propranolol at nanoscale liquid–liquid interface arrays, Anal. Chem. 87 (2015) 4487–4494.
[36] S. Amemiya, X. Yang, T.L. Wazenegger, Voltammetry of the phase transfer of polypeptide protamines across polarized liquid/liquid interfaces, J. Am. Chem. Soc. 125 (2003) 11832–11833.
[37] G. Pu, D. Zhang, X. Mao, Z. Zhang, H. Wang, X. Ning, X. Lu, Biomimetic interfacial electron-induced electrochemiluminesence, Anal. Chem. 90 (2018) 5272–5279.
[38] P.S. Toth, A.K. Rabiu, R.A.W. Dryfe, Controlled preparation of carbon nanotube-conducting polymer composites at the polarisable organic/water interface, Electrochem. Comm. 60 (2015) 153–157.
[39] D. Ibanez, D. Plana, A. Heras, D.J. Fermin, A. Colina, Monitoring charge transfer at polarisable liquid/liquid interfaces employing time-resolved raman spectroelectrochemistry, Electrochem. Comm. 54 (2015) 14–17.
[40] V. Mansfeldova, P. Janda, H. Tarabkova, J. Kaleta, Interface of two immiscible electrolytes as a potentiometric sensor for flow analysis, Anal. Lett. 49 (2016) 169–177.
[41] X. Lu, P. Sun, D. Yao, B. Wu, Z. Xue, X. Zhou, R. Sun, L. Li, X. Liu, Heterogeneous consecutive electron transfer at graphite electrodes under steady state, Anal. Chem. 82 (2010) 8598–8603.
[42] X. Lu, L. Hu, X. Wang, Thin-layer cyclic voltammetric and scanning electrochemical microscopic study of antioxidant activity of ascorbic acid at liquid/Liquid interface, Electroanalysis 17 (2005) 953–958.
[43] V. Sladkov, V. Guillou, S. Peulon, M. L'Her, Voltammetry of tetraalkylammonium picrates at water | nitrobenzene and water | dichloroethane microinterfaces; influence of partition phenomena, J. Electroanal. Chem. 573 (2004) 129–138.
[44] Y. Yatziv, I. Turyan, D. Mandler, A new approach to micropatterning: application of potential-assisted ion transfer at the liquid– liquid interface for the local metal deposition, J. Am. Chem. Soc. 124 (2002) 5618–5619.
[45] B. Liu, M.V. Mirkin, Electron transfer at liquid/liquid interfaces. The effects of ionic adsorption, electrolyte concentration, and spacer length on the reaction rate, J. Phys. Chem. B 106 (2002) 3933–3940.
[46] O. Valent, J. Koryta, M. Panoch, Voltammetric study of ion transfer across the water/o-nitrophenyloctyl ether interface: part I. Reversible process, J. Electroanal. Chem. 226 (1987) 21–25.
[47] S.M. Ulmeanu, H. Jensen, Z. Samec, G. Bouchard, P.-.A. Carrupt, H.H. Girault, Cyclic voltammetry of highly hydrophilic ions at a supported liquid membrane, J. Electroanal. Chem. 530 (2002) 10–15.
[48] S.M. Uleanu, H. Jensen, G. Bouchard, P.-.A. Carrupt, H.H. Girault, Water-oil partition profiling of ionized drug molecules using cyclic voltammetry and a 96-well microfilter plate system, Pharm. Res. 20 (2003) 1317–1322.
[49] M. Tsionsky, A.J. Bard, M.V. Mirkin, Scanning electrochemical microscopy. 34. Potential dependence of the electron-transfer rate and film formation at the liquid/liquid interface, J. Phys. Chem. 100 (1996) 17881–17888.

[50] A.L. Barker, P.R. Unwin, S. Amemiya, J. Zhou, A.J. Bard, Scanning electrochemistry microscopy (SECM) in the study of electron transfer kinetics at liquid/liquid interfaces: beyond the constant composition approximation, J. Phys. Chem. B 103 (1999) 7260–7269.
[51] N. Nishi, T. Kawakami, F. Shigematsu, M. Yamamoto, T. Kakiuchi, Fluorine-free and hydrophobic room-temperature ionic liquids, tetraalkylammonium bis(2-ethylhexyl)sulfosuccinates, and their ionic liquid–water two-phase properties, Green Chem. 8 (2006) 349–355.
[52] A.D. Ballantyne, A.K. Brisdon, R.A.W. Dryfe, Immiscible electrolyte systems based on asymmetric hydrophobic room temperature ionic liquids, Chem. Commun. (2008) 4980–4982.
[53] T.J. Stockmann, Z. Ding, Hydrophobicity of room temperature ionic liquids assessed by the Galvani potential difference established at micro liquid/liquid interfaces, J. Electroanal. Chem. 649 (2010) 23–31.
[54] D.S. Silvester, D.W.M. Arrigan, Array of water| room temperature ionic liquid micro-interfaces, Electrochem. Commun. 13 (2011) 477–479.
[55] E. Wang, Z. Sun, Ion transfer of bromocresol green across liquid-liquid interfaces, Anal. Chem. 59 (1987) 1414–1417.
[56] Z. Sun, E. Wang, Some solvents and supporting electrolytes studied for electrochemical measurement at liquid/liquid interface, Electroanalysis 1 (1989) 507–515.
[57] Y. Wang, T. Kakiuchi, Y. Yasui, M.V. Mirkin, Kinetics of ion transfer at the ionic liquid/water nanointerface, J. Am. Chem. Soc. 132 (2010) 16945–16952.
[58] P. Jing, M. Zhang, H. Hu, X. Xu, Z. Liang, B. Li, L. Shen, S. Xie, C.M. Pereira, Y. Shao, Ion-transfer reactions at the nanoscopic water/n-octanol interface, Angew. Chem. Int. Ed. 45 (2006) 6861–6864.
[59] L.M. Diamante, T. Lan, Absolute viscosities of vegetable oils at different temperatures and shear rate range of 64.5 to 4835 s^{-1}, J. Food. Proc. (2014) 234583.
[60] C. Tangsathitkulchai, Y. Sittichaitaweekul, M. Tangsathitkulchai, Temperature effect on the viscosities of palm oil and coconut oil blended with diesel oil, J. Am. Oil Chem. Soc. 81 (2004) 401–404.
[61] J. Speight, Lange's Handbook of Chemistry, 17th edition, McGraw-Hill, New York, NY, 2017.
[62] A.J. Bard, L.R. Faulkner, Electrochemical Methods: Fundamentals and Applications (2nd ed), John Wiley & Sons, Inc, Hoboken, NJ07030
[63] M. Shen, Z. Qu, J. DesLaurier, T.M. Welle, J.V. Sweedler, R. Chen, Single synaptic observation of cholinergic neurotransmission on living neurons: concentration and dynamics, J. Am. Chem. Soc. 140 (2018) 7764–7768.
[64] T.M. Welle, K. Alanis, M.L. Colombo, J.V. Sweedler, M. Shen, A high spatiotemporal study of somatic exocytosis with scanning electrochemical microscopy and nanoITIES electrodes, Chem. Sci. 9 (2018) 4937–4941.
[65] M. Shen, R. Ishimatsu, J. Kim, S. Amemiya, Quantitative imaging of ion transport through single nanopores by high-resolution scanning electrochemical microscopy, J. Am. Chem. Soc. 134 (2012) 9856–9859.
[66] J. Kim, A. Izadyar, M. Shen, R. Ishimatsu, S. Amemiya, Ion permeability of the nuclear pore complex and ion-induced macromolecular permeation as studied by scanning electrochemical and fluorescence microscopy, Anal. Chem. 86 (2014) 2090–2098.
[67] J. Kim, M. Shen, N. Nioradze, S. Amemiya, Stabilizing nanometer scale tip–to-substrate gaps in scanning electrochemical microscopy using an isothermal chamber for thermal drift suppression, Anal. Chem. 84 (2012) 3489–3492.
[68] S.R. Puri, J. Kim, Kinetics of antimicrobial drug ion transfer at a water/oil interface studied by nanopipet voltammetry, Anal. Chem. 91 (2019) 1873–1879.
[69] C. Cai, Y. Tong, M.V. Mirkin, Probing rapid ion transfer across a nanoscopic liquid-liquid interface, J. Phys. Chem. B 108 (2004) 17872–17878.
[70] P.J. Rodgers, S. Amemiya, Y. Wang, M.V. Mirkin, Nanopipet voltammetry of common ions across the liquid– liquid interface. Theory and limitations in kinetic analysis of nanoelectrode voltammograms, Anal. Chem. 82 (2010) 84–90.
[71] Y. Wang, J. Velmurugan, M.V. Mirkin, P.J. Rodgers, J. Kim, S. Amemiya, Kinetic study of rapid transfer of tetraethylammonium at the 1, 2-dichloroethane/water interface by nanopipette voltammetry of common ions, Anal. Chem. 82 (2010) 77–83.
[72] C.G. Zoski, M.V. Mirkin, Steady-state limiting currents at finite conical microelectrodes, Anal. Chem. 74 (2002) 1986–1992.
[73] P.J. Rodgers, S. Amemiya, Cyclic voltammetry at micropipet electrodes for the study of ion-transfer kinetics at liquid/liquid interfaces, Anal. Chem. 79 (2007) 9276–9285.
[74] B. Kralj, R.A. W.Dryfe, Hydrodynamic voltammetry at the liquid/liquid interface: the rotating diffusion cell, J. Phys. Chem. B 106 (2002) 6732–6739.
[75] Y. Yuan, Y. Shao, Systematic investigation of alkali metal ion transfer across the micro-and nano-water/1, 2-dichloroethane interfaces facilitated by dibenzo-18-crown-6, J. Phys. Chem. B 106 (2002) 7809–7814.
[76] A. Benvidi, S.N. Lanjwani, Z. Ding, Facilitated proton transfer by 2-acetylpyridine-4-phenyl-3-thiosemicarbazone across water/1, 2-dichloroethane interface, J. Electroanal. Chem. 641 (2010) 99–103.
[77] T. Kakiuchi, Current-potential characteristic of ion transfer across the interface between two immiscible electrolyte solutions based on the Nernst-Planck equation, J. Electroanal. Chem. 322 (1992) 55.
[78] K. Kontturi, J.A. Manzanares, L. Murtomaki, D.J. Schiffrin, Rate constant for ion transfer in inhomogeneous media at the interface of immiscible electrolytes, J. Phys. Chem. 101 (1997) 10801.
[79] W. Schmickler, A model for ion transfer through liquid| liquid interfaces, J. Electroanal. Chem. 426 (1997) 5–9.